ARTHRITIS & RHEUMATISM
Vol. 63, No. 10, October 2011, pp 3048–3057
DOI 10.1002/art.30458

Neuroimaging Evidence of White Matter Inflammation in Newly Diagnosed Systemic Lupus Erythematosus

Amy E. Ramage,[1] Peter T. Fox,[1] Robin L. Brey,[2] Shalini Narayana,[1] Matthew D. Cykowski,[3] Mohammad Naqibuddin,[4] Margaret Sampedro,[4] Stephen L. Holliday,[2] Crystal Franklin,[5] Daniel J. Wallace,[6] Michael H. Weisman,[6] and Michelle Petri[4]

***Objective*. Central nervous system (CNS) involvement occurs frequently in systemic lupus erythematosus (SLE) and frequently results in morbidity. The primary pathophysiology of CNS involvement in SLE is thought to be inflammation secondary to autoantibody-mediated vasculitis. Neuroimaging studies have shown hypometabolism (representing impending cell failure) and atrophy (representing late-stage pathology), but not inflammation. The purpose of this study was to detect the presence and regional distribution of inflammation (hypermetabolism) and tissue failure, apoptosis, or atrophy (hypometabolism).**

***Methods*. Eighty-five patients with newly diagnosed SLE, who had no focal neurologic symptoms, were studied. Disease activity was quantified using the Safety of Estrogens in Lupus Erythematosus: National Assessment version of the SLE Disease Activity Index (SELENA–SLEDAI), a validated index of SLE-related disease activity. ^{18}Fluorodeoxyglucose (FDG) positron emission tomography (PET) images of glucose uptake were analyzed by visual inspection and as group statistical parametric images, using the SELENA–SLEDAI score as the analysis regressor.**

***Results*. SELENA–SLEDAI–correlated increases in glucose uptake were found throughout the white matter, most markedly in heavily myelinated tracts. SELENA–SLEDAI–correlated decreases were found in the frontal and parietal cortex, in a pattern similar to that seen during visual inspection and presented in previous reports of hypometabolism.**

***Conclusion*. The SELENA–SLEDAI–correlated increases in glucose consumption are potential evidence of inflammation, consistent with prior reports of hypermetabolism in inflammatory disorders. To our knowledge, this is the first imaging-based evidence of SLE-induced CNS inflammation in an SLE inception cohort. The dissociation among ^{18}FDG uptake characteristics, spatial distribution, and disease activity correlation is in accordance with the notion that glucose hypermetabolism and hypometabolism reflect fundamentally different aspects of the pathophysiology of SLE with CNS involvement.**

Systemic lupus erythematosus (SLE), when present with central nervous system (CNS) symptoms, is characterized by a poorer prognosis, higher mortality rate (1), and reduced quality of life (2). The increased mortality and poor quality of life accompanying CNS involvement emphasize the importance of detecting SLE-mediated effects on the brain as early as possible. SLE, by best estimate, has a prevalence of ~350,000 cases in the US (3), with CNS involvement in as many as 80% of those (2,4). Within the first 2 years of disease, ~20% of patients report neuropsychiatric symptoms that are attributed to SLE (2). However, many patients (28–40%) report at least 1 neuropsychiatric episode before or during the first year after diagnosis (2).

Supported in part by the Brain CONECTIONS study (NIH grants R01-AR-049125 and AR-043727) and by the Johns Hopkins University General Clinical Research Center and the University of Texas Health Science Center at San Antonio Frederic C. Bartter General Clinical Research Center (grant M01-RR-01346).

[1]Amy E. Ramage, PhD, Peter T. Fox, MD, Shalini Narayana, PhD: University of Texas Health Science Center at San Antonio and Department of Veterans Affairs Heart of Texas Health Care Network, San Antonio; [2]Robin L. Brey, MD, FAAN, Stephen L. Holliday, PhD: Department of Veterans Affairs Heart of Texas Health Care Network, San Antonio; [3]Matthew D. Cykowski, MD: University of Texas Health Science Center at San Antonio and University of Oklahoma Health Sciences Center, Oklahoma City; [4]Mohammad Naqibuddin, MBBS, MPH, Margaret Sampedro, Michelle Petri, MD, MPH: Johns Hopkins University School of Medicine, Baltimore, Maryland; [5]Crystal Franklin, BS: University of Texas Health Science Center at San Antonio; [6]Daniel J. Wallace, MD, Michael H. Weisman, MD: Cedars-Sinai Medical Center/David Geffen School of Medicine, University of California, Los Angeles.

Address correspondence to Amy E. Ramage, PhD, UTHSCSA, Research Imaging Institute, 7703 Floyd Curl Drive, MSC 6240, San Antonio, TX 78229. E-mail: ramagea@uthscsa.edu.

Submitted for publication January 10, 2011; accepted in revised form May 12, 2011.

The primary pathophysiology of SLE is inflammation secondary to autoantibody-mediated effects on tissue, degeneration of small vessels, and vasculopathy (5). Inflammation is initiated by circulating autoantibodies generating inflammation mediators and results in cell dysfunction, apoptosis, and tissue loss (1,5,6). Neuroimaging studies of SLE have provided extensive evidence of chronic changes indicative of late-stage pathology, and positron emission tomography (PET) studies have shown decreased blood flow (hypoperfusion) and decreased glucose metabolism (hypometabolism), chiefly in frontal and parietal gray matter. White matter volume loss and small punctate lesions have been demonstrated in T1- and T2-weighted magnetic resonance imaging (MRI) studies, and reduced myelination has been seen with diffusion-tensor MRI and magnetization transfer imaging, even in SLE patients with no clear structural damage (7). To date, the inciting pathology (i.e., inflammation) has not been detectable using neuroimaging methods.

In the present study, we used PET imaging to detect and localize both brain markers of inflammation (incipient pathology) and tissue failure and apoptosis (late-stage pathology) in patients with newly diagnosed, neurologically asymptomatic SLE. Using ^{18}F-fluorodeoxyglucose (^{18}FDG) PET, both inflammation (detected as increased ^{18}FDG uptake) and cell failure (detected as decreased ^{18}FDG uptake) were indexed. ^{18}FDG is commonly used to detect gray matter dysfunction and atrophy, because the glucose metabolic rate decreases as tissue failure worsens. However, ^{18}FDG can also be used to detect inflammation (e.g., vasculitis [8]), given that inflammatory cells demonstrate increased glucose transporter expression and that cytokines increase the affinity of glucose transporters for deoxyglucose (9). Methods similar to those used in the current study have been used to detect early evidence of white matter hypermetabolism in schizophrenia (10) and attention-deficit/hyperactivity disorder (11).

PET data can be analyzed by visual inspection, or more objectively by using regression methods to quantify covariance of regional ^{18}FDG uptake with a clinical measure (12). The Safety of Estrogens in Lupus Erythematosus: National Assessment modified version of the SLE Disease Activity Index (SELENA–SLEDAI) is a clinical measure used regularly in the evaluation of SLE (13) as an index of disease activity in multiple organs, including the brain. Its score correlates with the presence of punctate white matter lesions in the brain of SLE patients who do not have CNS signs or neuropsychiatric symptoms (14). The imaging analysis we utilized allows SELENA–SLEDAI scores to be used as a pattern vector to determine covariance of ^{18}FDG uptake with disease activity. We hypothesized that combining the in vivo assessment of inflammation or tissue failure in the brain with the SELENA–SLEDAI score would provide insight into the pathophysiology of CNS involvement in SLE.

PATIENTS AND METHODS

Patients. SLE patients meeting the revised classification criteria of the American College of Rheumatology (ACR) (15) were recruited into the study within 9 months of initial diagnosis. Patients were recruited from Johns Hopkins University School of Medicine in Baltimore (JHU), the University of Texas Health Science Center in San Antonio (UTHSCSA), and Cedars-Sinai Hospital in Los Angeles. The institutional review board at each site approved study procedures, and informed consent was obtained from all patients. One hundred fourteen patients were enrolled. Of those, 29 were excluded because they did not undergo baseline PET imaging (n = 18), did not have current SELENA–SLEDAI scores (n = 5), or had evidence of stroke (n = 6). Of the remaining 85 patients, 19 showed evidence of neuropsychiatric symptoms (NP+), and 17 had hyperintense white matter lesions or atrophy on MRI, as reported previously (16) (MRI+), consistent with a typical SLE inception cohort. However, to exclude any influence of prior neuropsychiatric symptoms or CNS involvement on the imaging results, we also analyzed the data using patients with no history of neuropsychiatric symptoms and no abnormalities on MRI (n = 49) (non-NP/MRI−).

Clinical data. Demographic, general clinical, and neurologic/neuropsychiatric information was recorded, and ACR neuropsychiatric SLE (NPSLE) case definitions (17) were assigned. The Automated Neuropsychological Assessment Metrics Test Battery (18) and a variety of traditional neuropsychological tests (i.e., California Verbal Learning Test [19], the Finger-Tapping Test [20], Wisconsin Card Sorting Test [21], Wechsler Adult Intelligence Scales [22], Digits Forward/Backward and Block Design subtests [verbal fluency] [23], and the Rey-Osterrieth Complex Figure [copy and delay] [24]) were administered to quantify cognitive function. A board-certified clinical neuropsychologist (SLH) made the determination of impairment on the neuropsychological tests, based on published age-corrected normative data for each test. Patient mood was assessed with the Calgary Depression Scale (25).

SLE activity was documented using the SELENA–SLEDAI. In addition, the Systemic Lupus International Collaborating Clinics/ACR Damage Index (SLICC/ACR) (26) was used to record irreversible changes in organ function present for at least 6 months.

Image acquisition. Two PET scans were obtained for each patient in a single scanning session (1 transmission scan and 1 ^{18}FDG emission scan). The 10-minute transmission scan used a ^{68}Ge/^{68}Ga rod source and was used for attenuation correction of the emission scan. A 20-minute emission scan was obtained following intravenous administration of 185–370 mBq (~5 mCi) of ^{18}FDG and a 30-minute uptake period, during which the patient rested with his or her eyes closed in a darkened room. Images were reconstructed by filtered back

projection, using site-specific filters, resulting in a single PET scan with average emission per voxel. At the image analysis site (UTHSCSA), all images were refiltered with a Gaussian kernel to a full width at half maximum of 7 mm isotropic and were value normalized to a whole-brain mean value of 1,000 PET counts, thus correcting for global differences in glucose metabolism across patients. Because PET counts and ^{18}FDG uptake are linearly correlated (27) and the data analyses were nonquantitative (visual inspection) or correlation based (voxel-wise analysis), images were not converted to glucose metabolic rate or standard uptake values.

Two high-resolution whole-brain MRI scans were obtained for each patient in a single scanning session in which one T1-weighted image and one T2-weighted image were obtained. Image parameters were as follows: for T1-weighted images, time to recovery (TR) 500 msec, echo time (TE) 20 msec, flip angle 90°; for T2-weighted images, TR 3,400 msec, TE 20–80 msec, flip angle 90°, using a dual echo pulse sequence. T1-weighted images from all study sites were used to visually assess atrophy. T1-weighted images from 2 sites (UTHSCSA, JHU) were obtained in 3-dimensional (3-D) mode and were suitable for spatial normalization of the PET images, as well as for assessment of atrophy. T2-weighted images were used to detect white matter lesions.

Image spatial normalization. Spatial normalization of PET images (alignment of the images to a known anatomic reference) is a prerequisite for the voxel-wise correlational analysis used in the present study. Because anatomic MR images were acquired in 3-D at 2 study sites (UTHSCSA and JHU) and in 2-D at 1 study site (Cedars-Sinai), spatial normalization steps differed between study sites. For spatial normalization of PET images obtained at UTHSCSA and JHU, each patient's MRI results were used as a reference. This method is preferred, as the anatomic features used for spatial normalization are more apparent in T1-weighted MR images than in PET images. For each patient, PET images were co-registered to the corresponding T1-weighted MR image (with tissue other than brain tissue removed from the image), with the anterior commissure as the origin and the midsagittal plane as the y–z plane, and in the dimension of the Talairach and Tournoux 1988 atlas using the FMRIB Software Library (FSL) Linear Image Registration Tool (28). For data obtained at Cedars-Sinai, PET images were normalized directly to a high-resolution anatomic image (29). Once in standard space, an average PET image was created separately for each study site, and each patient's normalized PET image was nonlinearly aligned to the site-specific average (30). After spatial normalization, PET images were resampled isotropically at $2 \times 2 \times 2$–mm voxel spacing, sinc interpolated, and smoothed to 15-mm full width at half maximum with a Hanning filter.

Voxel-wise correlation analysis. Whole brain voxel-wise analyses were computed for 4 patient groups: all patients (n = 85), the non-NP/MRI− group (n = 49), the MRI+ group (n = 17), and the NP+ group (n = 19). Two patients with neuropsychiatric symptoms also had abnormalities visible on MRI. For each patient group, correlation images were calculated in 2 stages. First, voxel-wise correlation images were computed to determine the pattern of ^{18}FDG uptake in relation to SELENA–SLEDAI score for each patient group within each study site. Second, these group-wise images were pooled across study sites. This 2-stage approach was taken to avoid introducing artifacts into the analysis by merging raw-format images from different PET scanners.

Within each group, T statistics were computed for all voxels in the image and a map was generated indicating the T value for each voxel, for each study site using the SELENA–SLEDAI score as a regressor, controlling for the effects of age. T statistics for images were computed using the FSL general linear model function (randomise [31]). Monte Carlo permutations (1,000 permutations per image) were computed to create a distribution of test statistics under the null hypothesis (no effect of SELENA–SLEDAI score), using an exact test for partial correlation.

T statistics for images from across study sites were computed by applying an unweighted Z analysis (32) to within-site images from each of the 3 study sites for each group, using MatLab routines. In this method, T score images derived from FSL randomise were normalized to Z score image maps. The Z score images for each study site were combined and normalized to create a single Z score image, representing the combined results across sites. Using this method, the null hypothesis may be rejected within the aggregate data even when the results may not be significant for any study site alone. The Z image was then converted to a 2-tailed probability map and a significance threshold of $Z > 3$ (representing $P < 0.002$) for clusters of >10 voxels (80 mm^3) was applied. Suprathreshold clusters are reported for both SELENA–SLEDAI–correlated increases and decreases in ^{18}FDG uptake. The peak coordinates for each significant cluster were labeled for specific anatomic location using Talairach Daemon (available at www.talairach.org), and tissue type (both white and gray matter) was verified by visual inspection.

Interpretation under blinded conditions. Three experienced readers concurrently rated all PET and MR images, achieving consensus for each reading. Images for each modality were read in independent sessions so that for PET, readers were blinded with regard to corresponding MRI results. Readers were also blinded with regard to patient diagnosis (with normal controls included as foils) and study site. Images were normalized to the cerebellum mean count. Readers saw the PET images in 3 color spectra: 1) spectrum mode using a range of 15–85% of the cerebellum mean, 2) grayscale mode using a range of 15–85%, and 3) spectrum mode using the full width. All 3 viewing modes were rated on a 4-point scale (0 = normal, 1 = mildly abnormal, 2 = moderately abnormal, 3 = severely abnormal). MRI results have previously been published (14) and are used here only for grouping PET data (e.g., MRI+ and MRI−) for analysis.

RESULTS

Patient demographics. This was an inception cohort in which all patients were enrolled within 9 months of first diagnosis. Patients showed mild to moderate SLE activity (mean ± SD SELENA–SLEDAI score 4 ± 4.5) and little irreversible tissue damage (mean ± SD SLICC/ACR Damage Index 0.7 ± 1.16), and were not depressed (mean ± SD Calgary Depression Scale 5 ± 4) and performed within normal limits on the Automated Neuropsychological Assessment Metrics

Table 1. Demographic and clinical characteristics of the patients with SLE*

Characteristic	All patients (n = 85)	Non-NP/MRI− (n = 49)	NP+ (n = 19)†	MRI+ (n = 17)
Age	40 ± 12	37 ± 12	41 ± 9	45 ± 13
Sex, no. of female patients	75	47	14	14
Ethnicity, no. of patients				
African American	10	6	3	1
Asian	4	4	0	0
Hispanic	17	8	3	7
American Indian	1	0	1	0
White non-Hispanic	52	29	12	12
Other	2	2	0	0
SELENA–SLEDAI score	3.83 ± 4.53	3.04 ± 3.76	5.37 ± 6.6	5.3 ± 6.6
SLICC/ACR Damage Index	0.65 ± 1.16	0.53 ± 1	1.26 ± 1.59	0.85 ± 1.42
Calgary Depression Scale	4.69 ± 4.3	4.91 ± 4.64	4.84 ± 4.85	4.5 ± 3.56
ANAM average z-throughput	0.02 ± 0.71	0.11 ± 0.67	−0.12 ± 0.77	−0.10 ± 0.74
Neuropsychological tests, no. of patients scoring >2 SDs below normal mean	21	11	6	4
Medications, % of patients				
Prednisone (12–240 mg/day)	45	32	63	55
Methylprednisolone (800–1,600 mg/day)	2	10	0	0
Hydroxychloroquine (800–1,600 mg/day)	81	72	79	95
Acetylsalicylic acid (80–1,600 mg/day)	8	2	21	10

* Except where indicated otherwise, values are the mean ± SD. There were no significant differences between patient groups. Age, sex, and race in this sample are representative of typical SLE populations (i.e., higher in young, female, African American, and Hispanic groups [1]). SLE = systemic lupus erythematosus; non-NP/MRI− = group of patients with no history of neuropsychiatric symptoms and no abnormalities on magnetic resonance imaging; NP+ = group of patients showing evidence of neuropsychiatric symptoms; MRI+ = group of patients with hyperintense white matter lesions or atrophy on MRI; SELENA–SLEDAI = Safety of Estrogens in Lupus Erythematosus: National Assessment version of the SLE Disease Activity Index; SLICC/ACR = Systemic Lupus International Collaborating Clinics/American College of Rheumatology; ANAM = Automated Neuropsychological Assessment Metrics.

† Two of the NP+ patients had abnormalities in periventricular white matter and 1 had mild atrophy evidenced on MRI.

(mean ± SD average z-throughput 0.02 ± 0.71) compared to age-matched normal subjects. Twenty-four patients scored >2 SD below the mean in an age-matched normative control group on at least 1 of the traditional neuropsychological tests, but only 3 patients scored as poorly on ≥2 of the tests.

Demographic and clinical features of the 85 SLE patients (age range 20–69 years) assessed across the 3 study sites are summarized in Table 1. Nine patients were experiencing an active, mild or moderate disease flare (i.e., current worsening symptoms as characterized by the SELENA–SLEDAI). The main clinical indications of SLE were arthritis (21 of the 85 subjects), rash (27 of 85), or positive serology (low complement or anti-DNA level) (33 of 85). NPSLE manifestations, including reports of anxiety, mood disorder, psychosis, mononeuropathy, or headache, were evident in 19 patients (NP+ group). In most of these patients, symptoms had been present for as many as 10 years prior to SLE diagnosis. Of the components of the SELENA–SLEDAI pertaining to the CNS in the NP+ group, only cranial neuropathy and psychosis were reported (in 1 patient each). Seventeen patients had abnormalities visible on MRI (MRI+ group; 12 with atrophy, 5 with hyperintense white matter lesions). The remaining 49 patients had no evidence of either NP symptoms or abnormal MRI findings (non-NP/MRI− group).

Voxel-wise correlational analysis. *SELENA–SLEDAI–correlated increases*. The extent of disease activity–correlated increases in ^{18}FDG uptake was much greater in white matter than gray matter (Figure 1). In the overall patient group, SELENA–SLEDAI–correlated increases were present in frontal, parietal, and occipital centrum semiovale, subcortical temporal and limbic white matter, cerebellar white matter, and in brain stem tracts (Table 2 and Figure 2). In the NP+ and MRI+ groups, the SELENA–SLEDAI–correlated hypermetabolic regions were more extensive in frontal and subcortical white matter, particularly evident in the corpus callosum. In contrast, in the non-NP/MRI− group, the SELENA–SLEDAI–correlated increases in ^{18}FDG uptake were limited to focal white matter abnormalities in subgyral frontal lobe, anterior cingulate (limbic), and corpus callosum (subcortical).

SELENA–SLEDAI–correlated decreases. Disease activity–correlated decreases in ^{18}FDG uptake were

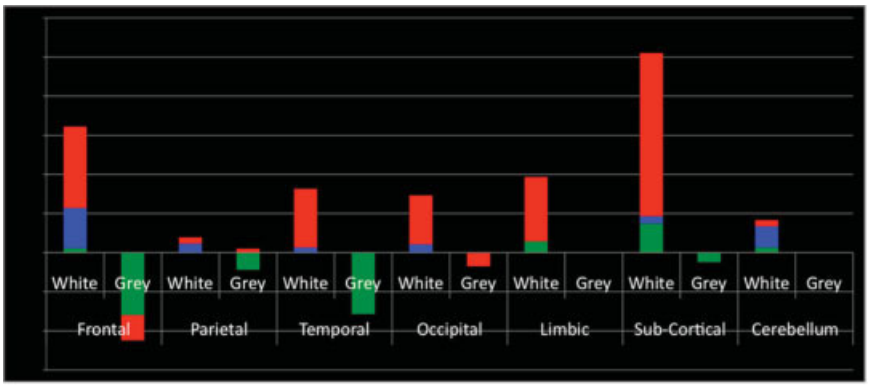

Figure 1. Representation of increases and decreases of ^{18}fluorodeoxyglucose (^{18}FDG) uptake in white and gray matter by patient group (patients with no history of neuropsychiatric symptoms and no abnormalities on magnetic resonance imaging [MRI] [non-NP/MRI−] [green], patients with hyperintense white matter lesions or atrophy on MRI [MRI+] [blue], and patients with neuropsychiatric symptoms [NP+] [red]) and brain area. Each lobe is differentiated by white and gray matter suprathreshold cluster extent, in mm^3. The NP+ group had the greatest extent of white matter effects. Gray matter effects, both increases and decreases, were limited in their extent and primarily occurred in the NP+ and non-NP/MRI− groups, except in the cerebellum, where all groups showed increased ^{18}FDG uptake.

quite limited in extent and occurred chiefly in gray matter (Table 2). For example, of the entire group, SELENA–SLEDAI–correlated decreases in ^{18}FDG uptake were limited to a small cluster in the middle frontal gyrus. Interestingly, the majority of SELENA–SLEDAI–correlated decreases in uptake occurred in the frontal

Table 2. Regions and coordinates for the largest z and cluster size seen in each group*

Location	Local maxima, z	Cluster size, mm^3	Standardized coordinates		
			x	y	z
Increase occurring in white matter					
Subgyral frontal					
All patients	3.7	664	−20	2	30
Non-NP/MRI−	3.41	88	36	28	16
NP+	4.22	480	22	36	−8
Subgyral temporal					
All patients	4.89	1,952	−32	−12	−10
NP+	3.61	328	24	−54	14
Anterior cingulate, non-NP/MRI−	3.87	232	−8	22	−2
Cingulate, NP+	3.99	376	−16	−10	26
Extranuclear					
All patients	3.87	160	−18	−52	20
NP+	4.25	352	16	−46	6
Non-NP/MRI−	4.5	456	−18	0	22
MRI+	4.09	152	22	−52	6
Corpus callosum					
All patients	3.57	80	12	20	16
Non-NP/MRI−	3.69	136	12	26	10
NP+	4.65	1,880	−10	24	8
Decrease occurring in gray matter					
Precentral gyrus					
Non-NP/MRI−	−3.81	104	−44	−14	52
NP+	−4.4	120	40	−18	60
Medial frontal gyrus, non-NP/MRI−	−3.55	80	−18	10	46
Postcentral gyrus, non-NP/MRI−	−3.91	184	50	−14	50
Precuneus, non-NP/MRI−	−3.54	88	44	−70	34
Superior temporal gyrus, non-NP/MRI−	−3.77	480	−46	−6	−2
Insula, non-NP/MRI−	−3.83	192	46	−14	4

* See Table 1 for definitions.

and temporal regions and were seen in the non-NP/MRI− and NP+ groups (Figure 2). In many cases, the local maximum for a SELENA–SLEDAI–correlated decrease cluster was in white matter, but the extent of the cluster was in gray matter.

Visual interpretation of PET images. Decreases in glucose uptake in cortical gray matter were readily apparent on visual inspection of PET images from 36 of 85 patients. All images from normal subjects included as foils were graded 0 by blinded readers. For the SLE patients, the scores measuring severity of decrease in glucose uptake were as follows: grade 0, 50 patients; grade 1, 24 patients; grade 2, 8 patients; grade 3, 3 patients (2 of whom were in the non-NP/MRI− group and 1 of whom was in the NP+ group, experiencing anxiety and psychosis 2 years prior to PET scanning) (Figure 3). Visually detected abnormalities were limited to the frontal and parietal cortex. No white matter hypermetabolism was reported; however, this is expected, given that white matter does not utilize glucose as extensively as gray matter and is therefore difficult to assess by visual inspection in ^{18}FDG PET and is only detectable with group-wise regression analyses, as described above. The PET scores did not correlate with the SELENA–SLEDAI score (r = 0.171); that is, patients who had more severe PET scores did not have higher disease activity scores. Following completion of the entire study, an unblinded reading (focused on patients with greatest disease activity [highest SELENA–SLEDAI score]) was performed to determine if hypermetabolism was visually detectable when specifically sought; hypermetabolism was not detectable in this analysis.

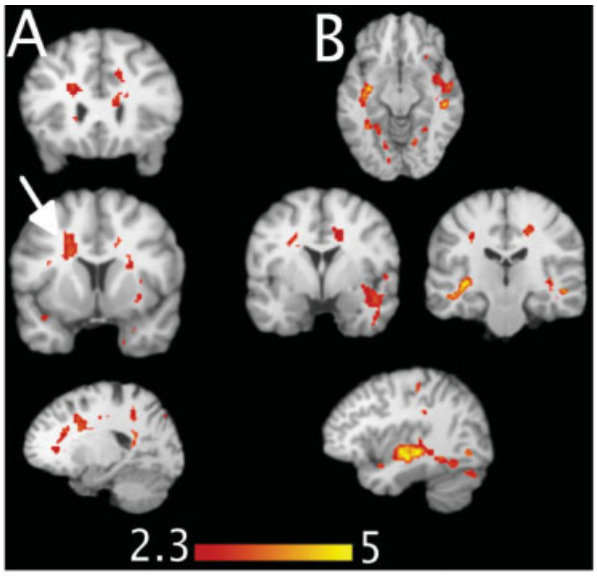

Figure 2. Increased ^{18}FDG uptake associated with Safety of Estrogens in Lupus Erythematosus: National Assessment version of the Systemic Lupus Erythematosus Disease Activity Index (SELENA–SLEDAI) score for the entire cohort. Large SELENA–SLEDAI–correlated clusters were observed in the frontal to parietal centrum semiovale (**A**) and bilateral temporal (**B**) white matter. The cluster of increased SELENA–SLEDAI–related ^{18}FDG uptake was also present in the group that had no evidence of either neuropsychiatric symptoms or abnormal MRI findings (**arrow**). See Figure 1 for other definitions.

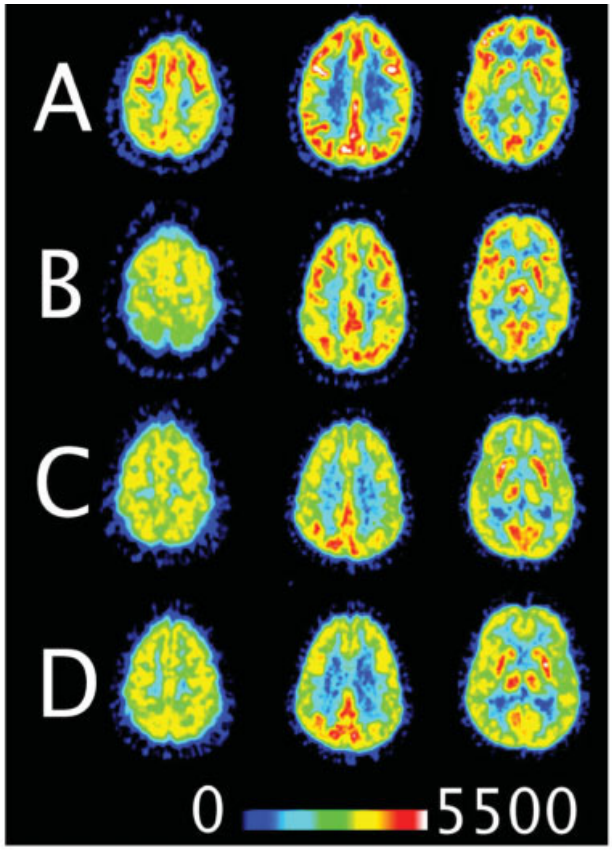

Figure 3. Visual analysis of raw positron emission tomography (PET) images from patients with systemic lupus erythematosus who had PET ratings of 0, indicating normal function (**A**), 1, indicating mild decrease in glucose uptake (**B**), 2, indicating moderate decrease in glucose uptake (**C**), and 3, indicating severe decrease in glucose uptake (**D**). The relative decrease of regions with high ^{18}fluorodeoxyglucose uptake is shown in red, and greater regions of low glucose uptake are shown in green ranging to blue. Mild ratings tended to be associated with either bifrontal or biparietal decreases (hypometabolism). Subcortical gray matter regions showed metabolic deficits across all subjects.

DISCUSSION

Widespread regional increases and decreases in brain glucose uptake were found in an inception cohort of SLE patients. While decreases in brain glucose metabolism (33) and perfusion (34) have previously been

reported in SLE, this is, to our knowledge, the first report of regional hypermetabolism. Although both hypermetabolism and hypometabolism were detected, the 2 phenomena differed markedly in their severity, spatial distribution, and correlation with systemic disease activity. Decreases in glucose consumption were quite distinct, being readily apparent to visual inspection, even on single-subject images (Figure 3). Hypometabolism was most marked in the frontal and parietal cortex, a finding that is consistent with those described in prior reports (33). Increases in glucose uptake were undetectable by visual inspection of per-patient images, and were only detected by group-wise regression analysis. SELENA–SLEDAI–correlated increases in ^{18}FDG uptake were diffusely present in white matter, and particularly dramatic in heavily myelinated tracts, including the centrum semiovale, corpus callosum, and internal capsule (Figure 2). Hypometabolism was minimally correlated with systemic disease activity, as defined by the SELENA–SLEDAI, while hypermetabolism was highly correlated with SELENA–SLEDAI score. This triple dissociation (severity, spatial distribution, and correlation with systemic disease activity) is strongly in accordance with the notion that glucose hypermetabolism and hypometabolism reflect fundamentally different aspects of the pathophysiology of CNS involvement in SLE.

The observed SELENA–SLEDAI–correlated white matter hypermetabolism is possible evidence of acute inflammation. In the CNS, evidence of inflammation has been found in SLE through postmortem histologic examinations, which reveal vasculitis, microinfarcts, and perivascular microglia surrounding small blood vessels (35). Antigens and autoantibodies, which are known to be elevated in the cerebrospinal fluid in SLE (36), generate the inflammation mediators interferon-α, interferon-inducible 10-kd protein (CXCL10), interleukin-6 and -8, and monocyte chemotactic protein 1 (37), which amplify inflammation and activate microglia (38). As noted above, inflammation increases glucose transporter expression, while cytokines increase the affinity of glucose transporters for deoxyglucose (9). Thus, increased uptake of ^{18}FDG would be expected in the presence of inflammation. That the glucose hypermetabolism was specifically correlated with systemic disease activity suggests that inflammatory activity levels in the CNS are influenced by systemic activity, even in the non-NP/MRI− group. Perhaps the most striking aspect of this finding is its spatial distribution; inflammatory activity in the CNS detected by glucose hypermetabolism was seen virtually entirely in white matter, but was diffuse.

Structural neuroimaging has provided ample evidence of white matter damage in SLE. Punctate white matter lesions and volume loss are common in periventricular and subcortical brain regions in SLE (39). Diffusion tensor imaging used in SLE has shown loss of white matter tissue integrity in limbic regions as well as in the insula, thalamus, corpus callosum, and parietal and frontal white matter (7,40). These findings are more common in NPSLE and in the chronic state of disease (41).

Some reports of white matter integrity in SLE as seen on structural MRI have suggested inflammatory changes. Appenzeller and colleagues used proton (hydrogen-1) magnetic resonance spectroscopy to detect impaired axonal integrity in occipitoparietal white matter prior to the appearance of focal white matter lesions or cortical atrophy, and concluded that atrophy is the consequence of a prior inflammatory process in SLE (42). Similarly, Bosma et al, using magnetization transfer ratio, detected subtle, diffuse white matter changes in SLE patients with neuropsychiatric symptoms as well as in those without neuropsychiatric symptoms during a symptomatic flare, but not in SLE patients without neuropsychiatric symptoms who were not experiencing disease flare; this is strongly indicative that a flare may be needed to cause white matter damage (43). Collectively, these findings suggest that white matter inflammation is a primary or early pathology in SLE, while punctate lesions and diffuse volume loss develop over time.

Numerous functional imaging studies have demonstrated gray matter functional decline in SLE. Consistently, ^{18}FDG PET, $H_2{}^{15}0$ PET, and ^{99m}technetium–hexamethylpropylene amine oxime—single-photon–emission computed tomography have shown cortical gray matter hypometabolism and hypoperfusion (44), in the same frontoparietal distribution observed in the present study. Considering the evidence that the incipient pathology in SLE consists of white matter inflammation followed by white matter lesions and volume loss, the gray matter specificity of the chronic hypometabolism and hypoperfusion requires explanation.

One potential explanation is that gray matter functional decline is a form of disconnection-induced diaschisis, in which diffuse loss of white matter structural integrity causes diffuse cortical functional decline in regions remote from, but connected to, other regions via these white matter tracts (45). In the other reports on functional imaging, diaschisis is most commonly associated with a focal, mixed-tissue (gray and white matter) lesion in one region causing a remote functional decline in a connected region. For example, a left frontal-lobe stroke will cause right cerebellar diaschisis (46). Small

ischemic white matter lesions, however, can also produce extensive cortical diaschisis in the area to which the fibers with lesions project (47). Similarly, decline in white matter integrity observed with normal aging results in decreased metabolism of glucose in cortical gray matter, and accounts for age-related cognitive decline (48). In SLE, the diffuse hypometabolism in gray matter may indicate the extensive nature of the white matter pathology, rather than indicting primary gray matter pathology.

The behavioral consequences of diaschisis are not well known. Remote diaschisis (e.g., cerebral–cerebellar) has been reported to resolve over time, but is not well correlated with behavioral recovery. Regions showing diaschisis do not always show later atrophy (47). Whether diaschisis due to undercutting white matter lesions is associated with gray matter volume loss is unknown. In a prior study, we found that volume loss on MRI (as determined by visual inspection) was present in ~25% of SLE subjects within 9 months of diagnosis (16). By visual analysis, however, it was impossible to determine whether the tissue loss was limited to white matter volume loss or included cortical thinning. Measuring cortical thickness with high-resolution structural MRI (T1-weighted) would best answer this question.

We presume that the regions of decreased SELENA–SLEDAI–correlated ^{18}FDG uptake in gray matter are indicative of potential tissue failure or diaschisis, but not loss, as a result of impaired white matter function due to inflammation. The cascade of inflammatory antibody/autoantibody release seen in SLE can mediate CNS tissue diaschisis (5). For example, circulating autoantibodies in SLE can bind to neuronal membranes, causing transient disruptions in cell function without lethal effects (49). In addition, antibodies may bind to endothelial cells in the vascular wall, thereby influencing the blood–brain barrier and allowing inflammatory agents to enter the CNS (50). It is known that indicators of inflammation (i.e., serum autoantibodies and histopathologically confirmed microinfarcts) are seen in SLE patients who do not have CNS signs or symptoms (35,51). In fact, the timeline in SLE may be that serum markers are present 10 years prior to diagnosis of SLE, and they are likely to be present 1.5 years prior to any symptoms of disease (51).

Thus, SLE may be a silent disease for several years prior to diagnosis, with the potential for white matter inflammation transiently causing diaschisis in gray matter (6). The remitting and recurring nature of SLE may allow regions that are frequently exposed to the inflammation cascade to ultimately fail, resulting in apoptosis and atrophy; this could be verified only with a longitudinal study. Based on our data, we hypothesize that the CNS becomes involved early in the course of SLE, prior to severe systemic medical symptoms, suggesting that SLE manifestations and concomitant systemic inflammation play an important early role in SLE-related brain pathophysiology.

We have shown a strong association between SLE disease activity and increased ^{18}FDG uptake, indicating inflammation in the white matter of patients with newly diagnosed SLE. Consistent with the findings in other studies, we also found decreased ^{18}FDG uptake in frontal and parietal gray matter that was minimally correlated with disease activity. We propose that inflammation of white matter is the inciting pathology in the CNS and that gray matter tissue failure and subsequent apoptosis or atrophy represent late-stage pathology. Given the sensitivity of our measure in detecting CNS inflammation in newly diagnosed SLE, future study is necessary to further explore the underlying CNS pathophysiology, using other imaging metrics that are more sensitive to white matter integrity (e.g., diffusion tensor imaging) and to inflammation (e.g., ^{18}FDG PK11195 PET to detect microglial activation) very early in the disease progression. These techniques and our methods could also be used to follow the evolution and effect of inflammation on brain tissue during flares and remission, as well as to assess the efficacy of treatments to reduce inflammation and late-stage damage.

ACKNOWLEDGMENTS

The authors thank Dionicio Galarza, MD and Jorge Esquivel, MD, Universidad Autónoma de Nuevo León, Mexico, for referring patients for enrollment at the UTHSCSA site.

AUTHOR CONTRIBUTIONS

All authors were involved in drafting the article or revising it critically for important intellectual content, and all authors approved the final version to be published. Dr. Ramage had full access to all of the data in the study and takes responsibility for the integrity of the data and the accuracy of the data analysis.

Study conception and design. Ramage, Fox, Brey, Narayana, Naqibuddin, Sampedro, Holliday, Wallace, Weisman, Petri.

Acquisition of data. Fox, Brey, Narayana, Naqibuddin, Holliday, Wallace, Weisman, Petri.

Analysis and interpretation of data. Ramage, Fox, Brey, Narayana, Cykowski, Holliday, Franklin, Wallace, Weisman, Petri.

REFERENCES

1. Trysberg E, Nylen K, Rosengren LE, Tarkowski A. Neuronal and astrocytic damage in systemic lupus erythematosus patients with central nervous system involvement. Arthritis Rheum 2003;48: 2881–7.
2. Hanly JG, Urowitz MB, Su L, Bae SC, Gordon C, Wallace DJ, et al. Prospective analysis of neuropsychiatric events in an interna-

tional disease inception cohort of patients with systemic lupus erythematosus. Ann Rheum Dis 2010;69:529–35.
3. Helmick CG, Felson DT, Lawrence RC, Gabriel S, Hirsch R, Kwoh CK, et al. Estimates of the prevalence of arthritis and other rheumatic conditions in the United States. Part I. Arthritis Rheum 2008;58:15–25.
4. Ainiala H, Loukkola J, Peltola J, Korpela M, Hietaharju A. The prevalence of neuropsychiatric syndromes in systemic lupus erythematosus. Neurology 2001;57:496–500.
5. Santer DM, Yoshio T, Minota S, Moller T, Elkon KB. Potent induction of IFN-α and chemokines by autoantibodies in the cerebrospinal fluid of patients with neuropsychiatric lupus. J Immunol 2009;182:1192–201.
6. Appenzeller S, Faria A, Marini R, Costallat LT, Cendes F. Focal transient lesions of the corpus callosum in systemic lupus erythematosus. Clin Rheumatol 2006;25:568–71.
7. Hughes M, Sundgren PC, Fan X, Foerster B, Nan B, Welsh RC, et al. Diffusion tensor imaging in patients with acute onset of neuropsychiatric systemic lupus erythematosus: a prospective study of apparent diffusion coefficient, fractional anisotropy values, and eigenvalues in different regions of the brain. Acta Radiol 2007;48:213–22.
8. Bleeker-Rovers CP, Bredie SJ, van der Meer JW, Corstens FH, Oyen WJ. Fluorine 18 fluorodeoxyglucose positron emission tomography in the diagnosis and follow-up of three patients with vasculitis. Am J Med 2004;116:50–3.
9. Love C, Tomas MB, Tronco GG, Palestro CJ. FDG PET of infection and inflammation. Radiographics 2005;25:1357–68.
10. Buchsbaum MS, Buchsbaum BR, Hazlett EA, Haznedar MM, Newmark R, Tang CY, et al. Relative glucose metabolic rate higher in white matter in patients with schizophrenia. Am J Psychiatry 2007;164:1072–81.
11. Fayed N, Modrego PJ. Comparative study of cerebral white matter in autism and attention-deficit/hyperactivity disorder by means of magnetic resonance spectroscopy. Acad Radiol 2005;12:566–9.
12. Fox PT, Ingham RJ, Ingham JC, Zamarripa F, Xiong JH, Lancaster JL. Brain correlates of stuttering and syllable production. A PET performance-correlation analysis. Brain 2000;123:1985–2004.
13. Petri M. Disease activity assessment in SLE: do we have the right instruments? Ann Rheum Dis 2007;66 Suppl 3:iii61–4.
14. Podrazilova L, Peterova V, Olejarova M, Tegzova D, Krasensky J, Seidl Z, et al. Magnetic resonance volumetry of pathological brain foci in patients with systemic lupus erythematosus. Clin Exp Rheumatol 2008;26:604–10.
15. Hochberg MC, for the Diagnostic and Therapeutic Criteria Committee of the American College of Rheumatology. Updating the American College of Rheumatology revised criteria for the classification of systemic lupus erythematosus [letter]. Arthritis Rheum 1997;40:1725.
16. Petri M, Naqibuddin M, Carson KA, Wallace DJ, Weisman MH, Holliday SL, et al. Brain magnetic resonance imaging in newly diagnosed systemic lupus erythematosus. J Rheumatol 2008;35:2348–54.
17. ACR Ad Hoc Committee on Neuropsychiatric Lupus Nomenclature. The American College of Rheumatology nomenclature and case definitions for neuropsychiatric lupus syndromes. Arthritis Rheum 1999;42:599–608.
18. Reeves D, Kane R, Winter K. Automated Neuropsychological Assessment Metrics (ANAM V3.11a/96) user's manual: clinical and neurotoxicology subset (Report No. NCRF-SR-96-01). San Diego: National Cognitive Foundation; 1996.
19. Delis DC, Kramer JH, Kaplan E, Ober BA. California verbal learning test, 2nd ed. Pearson; 2000.
20. Shimoyama I, Ninchoji T, Uemura K. The finger-tapping test: a quantitative analysis. Arch Neurol 1990;47:681–4.
21. Grant DA, Berg EA. Wisconsin Card Sorting Test (WCST). Pittsburgh: Western Psychological Services.
22. Wechsler D. Wechsler Adult Intelligence Scales: WAIS-IV. Pearson/Psychcorp 2008.
23. Lezak MD. Neuropsychological Assessment. Oxford: Oxford University Press; 1995.
24. Meyers JE, Meyers KR. Rey complex figure test and recognition trial professional manual. PAR.
25. Addington D, Addington J, Schissel B. A depression rating scale for schizophrenics. Schizophr Res 1990;3:247–51.
26. Dayal NA, Gordon C, Tucker L, Isenberg DA. The SLICC damage index: past, present and future. Lupus 2002;11:261–5.
27. Reivich M, Kuhl D, Wolf A, Greenberg J, Phelps M, Ido T, et al. Measurement of local cerebral glucose metabolism in man with ^{18}F-2-fluoro-2-deoxy-d-glucose. Acta Neurol Scand Suppl 1977;64:190–1.
28. Jenkinson M, Bannister PR, Brady JM, Smith SM. Improved optimisation for the robust and accurate linear registration and motion correction of brain images. Neuroimage 2002;17:825–41.
29. Kochunov P, Lancaster J, Thompson P, Toga AW, Brewer P, Hardies J, et al. An optimized individual target brain in the Talairach coordinate system. Neuroimage 2002;17:922–7.
30. Woods RP, Grafton ST, Holmes CJ, Cherry SR, Mazziotta JC. Automated image registration: I. General methods and intrasubject, intramodality validation. J Comput Assist Tomogr 1998;22:139–52.
31. Nichols TE, Holmes AP. Nonparametric permutation tests for functional neuroimaging: a primer with examples. Hum Brain Mapp 2002;15:1–25.
32. Lazar NA, Luna B, Sweeney JA, Eddy WF. Combining brains: a survey of methods for statistical pooling of information. Neuroimage 2002;16:538–50.
33. Kao CH, Ho YJ, Lan JL, Changlai SP, Liao KK, Chieng PU. Discrepancy between regional cerebral blood flow and glucose metabolism of the brain in systemic lupus erythematosus patients with normal brain magnetic resonance imaging findings. Arthritis Rheum 1999;42:61–8.
34. Driver CB, Wallace DJ, Lee JC, Forbess CJ, Pourrabbani S, Minoshima S, et al. Clinical validation of the watershed sign as a marker for neuropsychiatric systemic lupus erythematosus. Arthritis Rheum 2008;59:332–7.
35. Johnson RT, Richardson EP. The neurological manifestations of systemic lupus erythematosus. Medicine (Baltimore) 1968;47:337–69.
36. Zandman-Goddard G, Chapman J, Shoenfeld Y. Autoantibodies involved in neuropsychiatric SLE and antiphospholipid syndrome. Semin Arthritis Rheum 2007;36:297–315.
37. Fragoso-Loyo H, Richaud-Patin Y, Orozco-Narvaez A, Davila-Maldonado L, Atisha-Fregoso Y, Llorente L, et al. Interleukin-6 and chemokines in the neuropsychiatric manifestations of systemic lupus erythematosus. Arthritis Rheum 2007;56:1242–50.
38. Mondal TK, Saha SK, Miller VM, Seegal RF, Lawrence DA. Autoantibody-mediated neuroinflammation: pathogenesis of neuropsychiatric systemic lupus erythematosus in the NZM88 murine model. Brain Behav Immun 2008;22:949–59.
39. Appenzeller S, Vasconcelos Faria A, Li LM, Costallat LT, Cendes F. Quantitative magnetic resonance imaging analyses and clinical significance of hyperintense white matter lesions in systemic lupus erythematosus patients. Ann Neurol 2008;64:635–43.
40. Emmer BJ, Veer IM, Steup-Beekman GM, Huizinga TW, van der Grond J, van Buchem MA. Tract-based spatial statistics on diffusion tensor imaging in systemic lupus erythematosus reveals localized involvement of white matter tracts. Arthritis Rheum 2010;62:3716–21.
41. Sabbadini MG, Manfredi AA, Bozzolo E, Ferrario L, Rugarli C, Scorza R, et al. Central nervous system involvement in systemic lupus erythematosus patients without overt neuropsychiatric manifestations. Lupus 1999;8:11–9.
42. Appenzeller S, Li LM, Costallat LT, Cendes F. Neurometabolic changes in normal white matter may predict appearance of hyperintense lesions in systemic lupus erythematosus. Lupus 2007;16:963–71.

43. Bosma GP, Middelkoop HA, Rood MJ, Bollen EL, Huizinga TW, van Buchem MA. Association of global brain damage and clinical functioning in neuropsychiatric systemic lupus erythematosus. Arthritis Rheum 2002;46:2665–72.
44. Kao CH, Lan JL, ChangLai SP, Liao KK, Yen RF, Chieng PU. The role of FDG-PET, HMPAO-SPET and MRI in the detection of brain involvement in patients with systemic lupus erythematosus. Eur J Nucl Med 1999;26:129–34.
45. Feeney DM, Baron JC. Diaschisis. Stroke 1986;17:817–30.
46. Liu Y, Karonen JO, Nuutinen J, Vanninen E, Kuikka JT, Vanninen RL. Crossed cerebellar diaschisis in acute ischemic stroke: a study with serial SPECT and MRI. J Cereb Blood Flow Metab 2007;27:1724–32.
47. Mohr JP. Historical observations on functional reorganization. Cerebrovasc Dis 2004;18:258–9.
48. Kochunov P, Ramage AE, Lancaster JL, Robin DA, Narayana S, Coyle T, et al. Loss of cerebral white matter structural integrity tracks the gray matter metabolic decline in normal aging. Neuroimage 2009;45:17–28.
49. Scolding NJ, Joseph FG. The neuropathology and pathogenesis of systemic lupus erythematosus. Neuropathol Appl Neurobiol 2002; 28:173–89.
50. Kowal C, Degiorgio LA, Lee JY, Edgar MA, Huerta PT, Volpe BT, et al. Human lupus autoantibodies against NMDA receptors mediate cognitive impairment. Proc Natl Acad Sci U S A 2006; 103:19854–9.
51. Arbuckle MR, McClain MT, Rubertone MV, Scofield RH, Dennis GJ, James JA, et al. Development of autoantibodies before the clinical onset of systemic lupus erythematosus. N Engl J Med 2003;349:1526–33.